Stress-induced upper crustal anisotropy in southern California

Zhaohui Yang,[1,2] Anne Sheehan,[1,2] and Peter Shearer[3]

Received 27 April 2010; revised 5 November 2010; accepted 23 November 2010; published 5 February 2011.

[1] We use an automated method to analyze shear wave splitting from local earthquakes recorded by the Southern California Seismic Network between 2000 and 2005. The observed fast directions of upper crustal anisotropy generally are consistent with the direction of maximum horizontal compression σ_{Hmax}, suggesting that one major mechanism of anisotropy in the top 20 km of crust under southern California is regional stress. However, at other stations, fast directions are aligned with the trends of regional faulting and local alignment of anisotropic bedrock. Splitting delay times range widely within 0.2 s. These upper crustal anisotropy observations, together with previous studies of SKS shear wave splitting, surface waves, and receiver functions, suggest different mechanisms of anisotropy at different depths under southern California. Anisotropy in the upper crust appears to be in response to the current horizontal maximum compression σ_{Hmax}, which differs from the cause of anisotropy in the lower crust and mantle. We also explore possible temporal variations in upper crustal anisotropy associated with preearthquake stress changes or stress changes excited by surface waves of great earthquakes but do not observe any clear temporal variations in fast directions or time delays.

Citation: Yang, Z., A. Sheehan, and P. Shearer (2011), Stress-induced upper crustal anisotropy in southern California, *J. Geophys. Res.*, *116*, B02302, doi:10.1029/2010JB007655.

1. Introduction

[2] Measuring the depth distribution of seismic anisotropy in the lithosphere is an important tool for estimating the deformation history and the state of stress of a region. Observations of teleseismic shear wave splitting are common in studies of upper mantle anisotropy. Shear wave splitting from local earthquakes has also been utilized and gives constraints on anisotropy in the upper crust. Extensive studies of shear wave splitting from local earthquakes have been conducted in southern California [*Aster et al.*, 1990; *Aster and Shearer*, 1992; *Liu et al.*, 1997; *Cochran et al.*, 2003, 2006; *Boness and Zoback*, 2004, 2006; *Paulssen*, 2004; *Liu et al.*, 2008] and other active fault zone regions (e.g., Anatolian Fault [*Peng and Ben-Zion*, 2004]), which investigate the spatial distribution and possible temporal variations of crustal anisotropy.

[3] Crustal anisotropies could be caused by different mechanisms, which *Boness and Zoback* [2006] categorized into two main types. One is stress-induced anisotropy, which responds to the local tectonic stress. In this model, the medium consists of vertically aligned, fluid-filled microcracks parallel to the direction of maximum horizontal compressive stress σ_H [e.g., *Crampin*, 1978, 1987; *Leary et al.*, 1990], or the preferential closure of fractures in a randomly fractured crust [*Boness and Zoback*, 2004]. The other category is structural anisotropy due to rock or mineral fabric, such as preferential mineral alignment [*Brocher and Christensen*, 1990], rock fabric [*Kern and Wenk*, 1990], and remnant features of paleostress [e.g., *Aster and Shearer*, 1992].

[4] In the first case, when shear waves travel through the medium, vertically propagating shear waves are polarized with a fast direction parallel to the open microcracks [*Crampin*, 1986] or perpendicular to the closed macroscopic fractures [*Boness and Zoback*, 2004]. In the second case, vertically propagating shear waves will have a fast polarization parallel to the structural fabric, e.g., local shear wave splitting aligned with regional faulting [*Savage et al.*, 1990]. As it contains several active fault systems (e.g., San Andreas, San Jacinto, and Elsinore fault zones, Figure 1) and different geologic provinces, southern California is a good place to explore the spatial distribution of these two models, both of which could potentially be observed.

[5] Whether temporal variations in local splitting patterns can be a tool of monitoring stress changes for earthquake prediction has been debated for some time [e.g., *Aster et al.*, 1990; *Crampin et al.*, 1990]. More recently, temporal variations in local shear wave splitting have been found to correlate with volcanic activity and are being investigated as a forecasting tool for volcano eruptions [*Miller and Savage*, 2001; *Gerst and Savage*, 2004]. This revives interest in investigating the potential of using shear wave splitting from local earthquakes to monitor preearthquake stress changes or stress changes excited by passing surface waves. The long-term permanent seismograph stations available in southern

[1]Department of Geological Sciences, University of Colorado, Boulder, Colorado, USA.
[2]Cooperative Institute for Research in Environmental Sciences, University of Colorado at Boulder, Boulder, Colorado, USA.
[3]Institute of Geophysics and Planetary Physics, Scripps Institution of Oceanography, La Jolla, California, USA.

0148-0227/11/2010JB007655

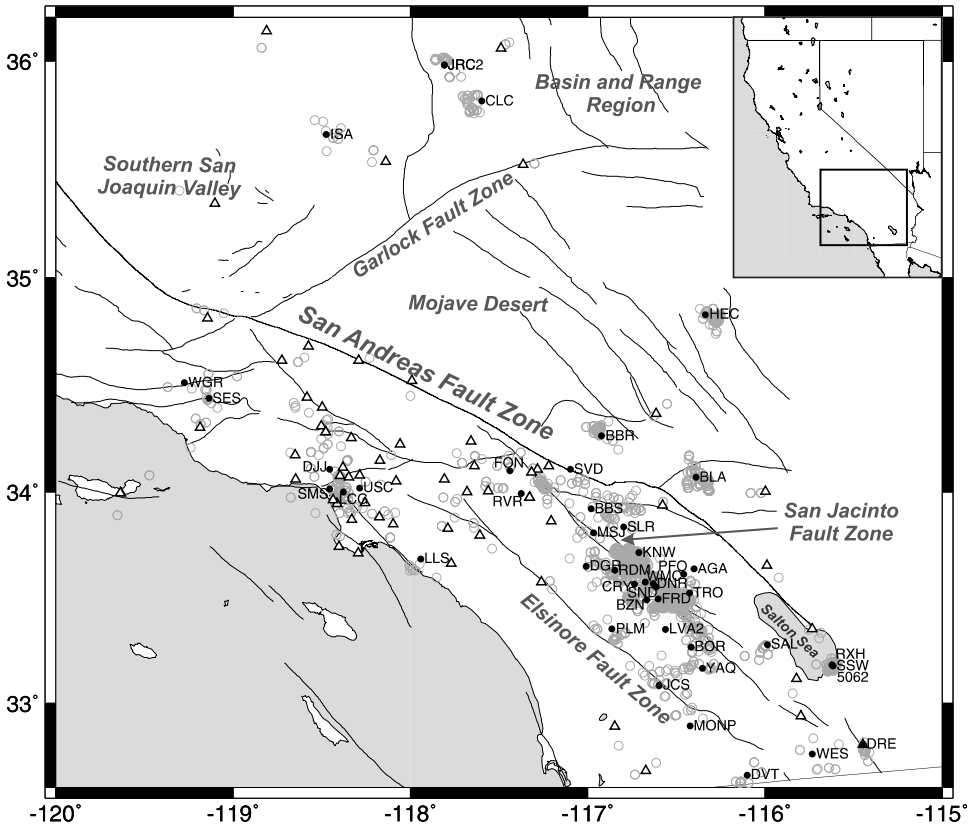

Figure 1. Map showing earthquakes (gray circles) used in this study and seismic stations that recorded the data (solid circles are the stations with results; open triangles are the stations without results fulfilling our selection criteria). Major late Quaternary faults [*Jennings*, 1994] are also shown on the map as thin lines.

California (Figure 1) make such temporal studies tractable, avoiding issues of differences in instrumentation or exact station location between temporary deployments.

[6] In this study, we take advantage of the dense Southern California Seismic Network (SCSN) (Figure 1) and its long-term continuous recordings to study upper crustal anisotropy in southern California. We report results at 45 stations with good quality measurements of local earthquake shear wave splitting in southern California. We compare the fast directions of our crustal anisotropy with the regional stress orientation, observed crustal anisotropy from teleseismic receiver functions, surface-wave studies, and results from SKS shear wave splitting. In addition, we search for possible temporal variations in anisotropy over a 5 year period.

2. Data and Method

[7] To study local shear wave splitting, we examine seismograms recorded by SCSN stations between 2000 and 2005, using a waveform database described by *Hauksson and Shearer* [2006]. The SCSN has several hundred stations and records about 12,000 to 35,000 earthquakes each year [*Shearer et al.*, 2006]. Our database includes both phase and waveform data from all available regional and local earthquakes. Traces are resampled to a uniform 100 Hz sample rate. The *S* waveforms from earthquakes are cut 1.5 s immediately before and after the picked times of the initial *S* arrivals.

[8] Local earthquake shear wave splitting uses shear waves from earthquakes close to the stations. When incidence angles at the surface are greater than 35°, converted phases can interfere with shear wave splitting measurements [*Booth and Crampin*, 1985; *Nuttli*, 1961]. To account for this, many researchers consider only events with incidence angles less than 45° based on straight-line raypaths (i.e., assuming homogeneous velocity) [e.g., *Peacock et al.*, 1988]. Although seismic waves with larger incidence angles have been used in some studies [*Paulssen*, 2004; *Savage et al.*, 2010], here we apply the 45° limit. The measured time delay between the fast and slow components represents the integrated anisotropy along the raypaths, which are between the crustal earthquake and the overlying seismic station. Because the earthquakes are fairly shallow (98.6% of earthquakes we use are above 20 km, Figure 2), these raypaths are mostly within the top 20 km of the crust.

[9] As the amount of data to be processed is very large, we utilize the method of *Teanby et al.* [2004] for automating the measurement of the shear wave splitting parameters ϕ (fast polarization direction) and δt (delay time). We perform the shear wave splitting correction based on the covariance matrix method [*Silver and Chan*, 1991]. This method determines the shear wave splitting parameters by constructing a 2×2 covariance matrix from the windowed horizontal components (Figures 2a and 2b) and minimizing the smaller eigenvalue λ_2 using a grid search over ϕ-δt space. The search range for ϕ is from $-90°$ to 90°. North is

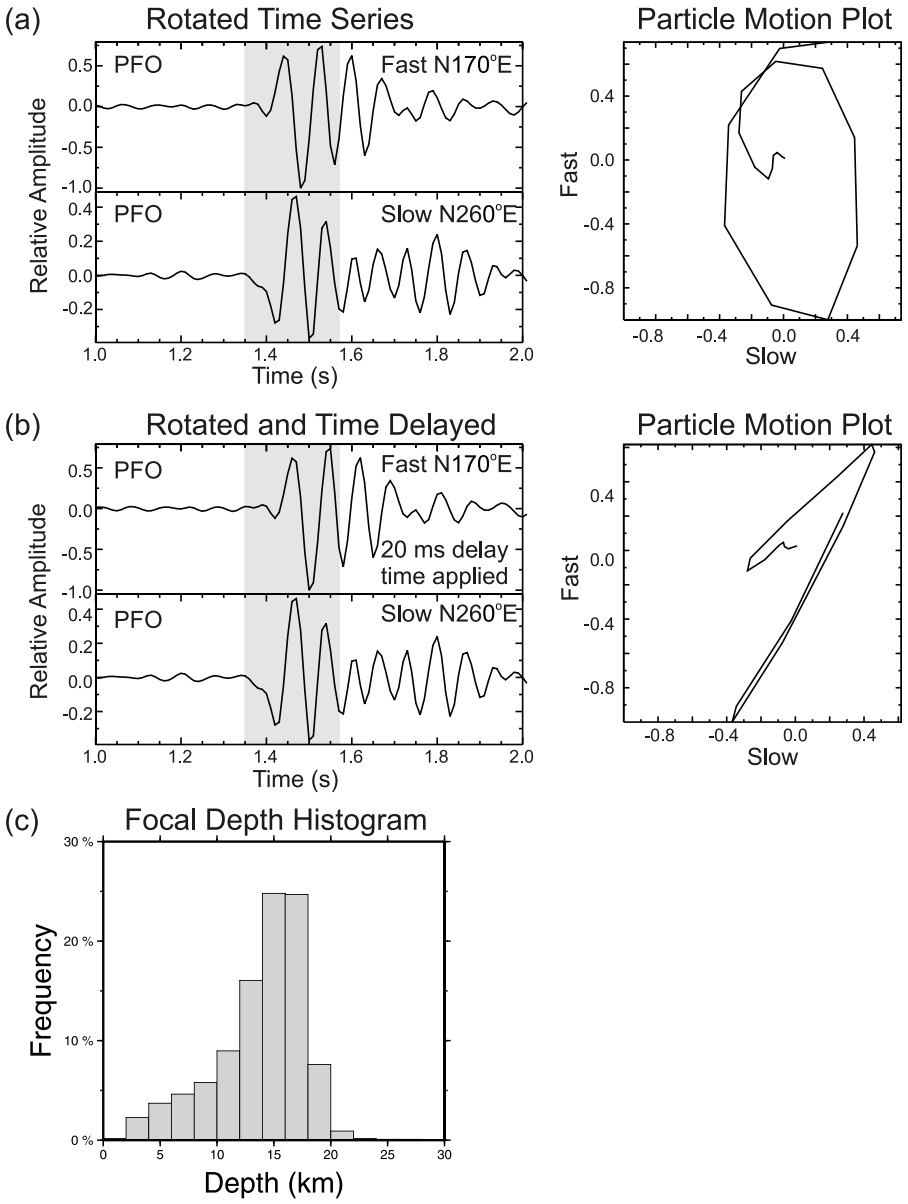

Figure 2. Examples of waveforms for one event at station PFO. (a) Horizontal seismograms rotated to fast (top trace) and slow (bottom trace) orientations. The *S* wave in the bottom trace arrives later by tens of milliseconds than that in the top trace. The particle motion plot on the right is from the shaded parts of the seismograms and shows an obvious elliptical motion. (b) A delay time of 20 ms has been applied to the fast component (top trace) to align the two shear wave arrivals. The particle motion plot now shows clear linearity. (c) Histogram showing the depth distribution of the earthquakes used in this study, which are mainly within the top 20 km.

defined as 0°, and the clockwise direction is positive. Splitting delay time δt is obtained by advancing the slow shear wave component by δt and rotating the fast and slow components into the initial polarization direction α, which is the direction of the eigenvector associated with the larger eigenvalue λ_1 of the covariance matrix. We use 0.2 s as the cutoff value for the time delay since previous studies show that the measured time delays for local earthquakes in southern California are less than 0.2 s [*Aster et al.*, 1990; *Boness and Zoback*, 2006].

[10] Prior to the analysis, the seismograms are bandpass filtered at 1–15 Hz, after the mean and trend are removed. As the dominant frequency for shear waves generated by local earthquakes ranges from about 5 to 10 Hz, this filter improves the signal-to-noise ratio without degrading the waveforms. To determine the shear wave splitting measuring window, we slide a 0.3 s time window around the first shear wave arrival with a step increment of 0.05 s between −0.1 and 0.35 s of the first *S* arrival. The best window is picked when the uncertainty of the fast direction is smallest.

[11] Because visual inspection of each measurement for quality control is not practical and could be subjective [e.g., *Aster et al.*, 1990; *Savage et al.*, 1990; *Gerst*, 2003], we apply the following criteria, similar to those used by *Peng*

and Ben-Zion [2004], to ensure reliability of results. We require (1) signal-to-noise ratio above 2.5, (2) maximum error of 20° for the fast orientation ϕ in the chosen measurement window, (3) initial polarization α not too close to the fast (or slow) orientation ϕ ($20 \leq | \phi - \alpha | \leq 70$), and (4) cross-correlation coefficient no less than 0.7. For the results presented here, we keep only the stations with more than three measurements that satisfy these criteria.

3. Results

[12] After applying the criteria described above, a total of 2190 high-quality measurements of fast directions at 45 seismograph stations are displayed using rose diagrams in Figure 3. The earthquakes used in these measurements are mainly from the top 20 km of the crust (Figure 2c). To provide a statistical analysis of the measured ϕ, we first multiply the fast direction angles by two to account for the bimodal nature of the distribution of fast directions (i.e., the 180° ambiguity) and then use the Von Mises method to calculate the mean angle θ and a mean resultant length R [*Davis*, 1986; *Mardia and Jupp*, 2000; *Cochran et al.*, 2003] (Table 1). The parameter R gives a quantitative estimate of the variance of the directional data, with values near 0 and 1 indicating high scattering and clustering, respectively.

[13] As shown in Figure 3, 30 of 45 stations have values of R with significance levels greater or equal to 90%, indicating that the ϕ values at these stations have a significant preferred direction. These stations occur over the entire area instead of concentrating in a specific region (Figure 4). Although some stations have R values with confidence levels less than 90%, the measurements nonetheless provide some indication of likely fast directions and may be useful in constraining spatial patterns in anisotropy in different directions (Figure 3, bottom plots).

[14] For the stations with significant preferred directions (Figure 3, stations labeled with an asterisk), the fast directions have a large north–south (N–S) component (except for stations BBS, PFO, RDM, SLR, and WGR), generally at azimuths between −30° and 30° (Figure 4, inset). At Anza, our results are fairly consistent with previous results from *Aster and Shearer* [1992] (Figure 4). Further to the north along the Hector Mine fault zone, *Cochran et al.* [2003] reported crustal anisotropy with fast directions ranging between N3°W and N12°E, roughly halfway between the fault strike and the direction of local stress vectors (Figure 4). The closest station in our study to their measurements is station HEC, which is located about 27 km north of the hypocenter of the 1999 Hector Mine earthquake (M 7.1). The fast directions at this station are N4°E ± 5°, consistent with the results of *Cochran et al.* [2003].

[15] Near the San Gabriel Mountains and the San Bernardino Mountains, the fast orientations of upper crustal anisotropy from *Paulssen* [2004] trend mostly N–S, generally consistent with our results. There are four measurements from *Paulssen* [2004] northwest of station BBS, subparallel to the local faults, trending WNW–ESE, having a large E–W component, that are roughly consistent with our results at station BBS (Figure 4). Station SVD has the largest value of standard error in its mean direction, which results from a bimodal distribution in only eight measurements. This station is located almost on top of the San Andreas Fault (SAF), yet it does not appear to have a strong fault-parallel fast direction (Figures 1 and 3). Paulssen's results close to this station also show a diversity of orientations (Figure 4).

4. Discussion

4.1. Comparison With Stress Vectors

[16] Southern California contains the southern part of the San Andreas Fault, which is the main transform plate boundary separating the Pacific and North American plates (Figure 1). The stress data in this region, which are based on focal mechanism solutions, borehole breakouts, and hydraulic fracturing experiments [*Heidbach et al.*, 2008], indicate an average orientation of N12°E for horizontal maximum compression σ_{Hmax} (Figure 4). In most regions, the average fast directions of crustal anisotropy from our study are subparallel to the direction of σ_{Hmax} (Figure 4, inset).

[17] Near the SAF (Banning Pass, the "Big Bend") and the San Jacinto Fault, the horizontal maximum compression σ_{Hmax} directions are mostly oriented within 10° from N–S (Figure 4). This orientation is about 60°–70° to the average strike of the SAF in southern California [*Townend and Zoback*, 2004]. No apparent stress rotations near the SAF are apparent at the scale of these stress observations [*Abers and Gephart*, 2001]. Stations in the Anza region have fast anisotropy directions similar to σ_{Hmax} (Figure 4) except for station KNW, which differs from the other stations in this region. Station KNW, located to the northeast of San Jacinto Fault, has 359 clustered measurements (R = 0.69) showing a fast direction trending NW–SE, subparallel to the fault trend. The measurements at station KNW all come from earthquakes with back azimuths between 180° and 270°. The fast direction at station KNW is likely due to a local alignment of anisotropic bedrock minerals, particularly biotite [*Aster and Shearer*, 1992]. Near the Big Bend of the SAF, the fast directions at stations BBS and SLR trend WNW–ESE and seem to be affected by the orientation of the Big Bend.

[18] Northeast of the SAF, stress data in the eastern California shear zone show that the horizontal maximum compression trends NE–SW (Figure 4), roughly perpendicular to a series of faults, such as the Calico, Emerson, and Lenwood faults. Station BBR near the San Bernardino Mountains shows a direction consistent with the regional stress vectors. Station HEC, which is to the east side of the shear zone and closer to the Landers rupture zone, has a large component parallel to the rupture zone, trending N4°E, agreeing with measurements from *Cochran et al.* [2003].

[19] In the west Los Angeles Basin, the direction of σ_{Hmax} is within 10° of N–S. The average fast orientations of anisotropy at stations LCG and USC are 18° and −23°, respectively (Figure 4). Although the measurements at DJJ and SMS have lower confidence levels in their preferred directions, the peaks in their rose diagrams seem to be consistent with those of LCG and USC. Further to the north in the Basin and Range region, the fast orientations and stress vectors are consistent, within 20° from north (Figure 4).

[20] For the stations with a significant preferred orientation, the rose diagrams of their mean fast directions have two prominent peaks. One peak falls within the range of the stress orientations of about −30° to 30° (Figure 4, inset). As discussed earlier, when the medium consists of microcracks or the preferential closure of fractures in a randomly

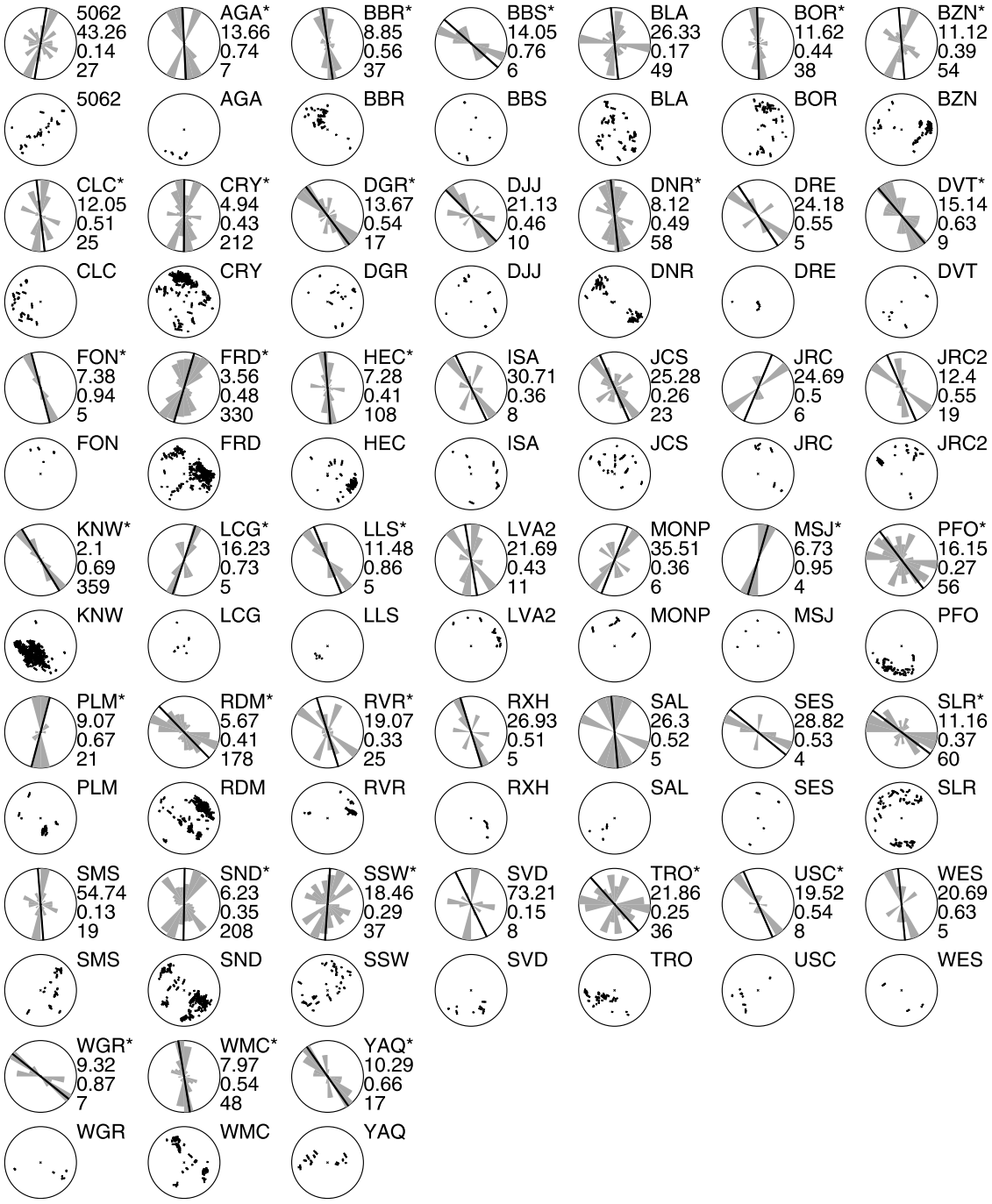

Figure 3. Normalized rose diagrams and stereonet projections of shear wave splitting measurements for the stations plotted as solid circles in Figure 1. Bin size is 15°, and the black line in each diagram is the average fast direction calculated as described in the text. The station name, the standard error of the mean direction (degrees), the *R* value, and the number of measurements are given to the right of each rose diagram. Stations labeled with an asterisk have significant preferred directions at the 90% confidence level.

fractured crust (often called stress-induced anisotropy), the resulting fast direction of shear wave splitting from vertically propagating shear waves is parallel to the maximum horizontal compressive stress σ_{Hmax}. Another less prominent peak around 45° seems to be subparallel to the trends of faults in this region (Figure 4). Therefore, our observations suggest that the bulk of upper crustal anisotropy (top 20 km) in southern California is due to stress-induced aligned cracks, whereas structural fabric is also a factor at some locations.

4.2. Comparison With SKS and Anisotropy From Receiver Functions

[21] Fast directions of SKS splitting observations are mostly E–W in southern California [e.g., *Polet and Kanamori*, 2002; *Liu et al.*, 1995; *Özalaybey and Savage*, 1995] (Figure 5).

Table 1. List of Station Information and Results

Station	Longitude	Latitude	Average Fast Direction	Standard Error	Average Delay Time	Standard Deviation	*R*	Number of Measurements
5062	−115.616	33.178	9.6	26.3	0.07	0.05	0.15	27
AGA[a]	−116.401	33.638	−2.8	8.3	0.05	0.04	0.74	7
BBR[a]	−116.921	34.262	−8.1	5.4	0.08	0.05	0.56	37
BBS[a]	−116.981	33.921	−48.2	8.5	0.05	0.05	0.76	6
BLA	−116.389	34.069	−5.9	16.0	0.1	0.04	0.18	49
BOR[a]	−116.417	33.268	−1.4	7.1	0.1	0.05	0.44	38
BZN[a]	−116.667	33.492	−4.6	6.8	0.09	0.05	0.39	54
CLC[a]	−117.598	35.816	−6.6	7.3	0.09	0.04	0.51	25
CRY[a]	−116.737	33.565	0.3	3.0	0.1	0.05	0.44	212
DGR[a]	−117.009	33.65	−36.9	8.3	0.06	0.05	0.54	17
DJJ	−118.455	34.106	−44.6	12.8	0.07	0.05	0.47	10
DNR[a]	−116.631	33.567	−6.0	4.9	0.09	0.05	0.50	58
DRE	−115.447	32.805	−33.6	14.7	0.08	0.05	0.56	5
DVT[a]	−116.101	32.659	−40.3	9.2	0.06	0.04	0.64	9
FON[a]	−117.439	34.1	−14.8	4.5	0.06	0.03	0.94	5
FRD[a]	−116.602	33.495	16.4	2.2	0.05	0.04	0.48	330
HEC[a]	−116.335	34.829	−4.4	4.4	0.07	0.04	0.42	108
ISA	−118.474	35.663	−25.4	18.7	0.13	0.05	0.37	8
JCS	−116.596	33.086	−23.9	15.4	0.08	0.05	0.27	23
JRC	−117.808	35.982	22.9	15.0	0.13	0.05	0.51	6
JRC2[a]	−117.809	35.982	−23.7	7.5	0.11	0.06	0.56	19
KNW[a]	−116.712	33.714	−31.4	1.3	0.09	0.04	0.70	359
LCG[a]	−118.378	34	18.4	9.9	0.07	0.02	0.74	5
LLS[a]	−117.943	33.685	−22.5	7.0	0.04	0.02	0.86	5
LVA2	−116.562	33.352	−9.5	13.2	0.1	0.04	0.44	11
MONP	−116.423	32.893	21.4	21.6	0.14	0.03	0.37	6
MSJ[a]	−116.968	33.808	16.3	4.1	0.05	0.01	0.96	4
PFO[a]	−116.459	33.612	−37.4	9.8	0.06	0.05	0.27	56
PLM[a]	−116.863	33.354	14.9	5.5	0.12	0.03	0.68	21
RDM[a]	−116.848	33.63	−44.1	3.4	0.09	0.05	0.42	178
RVR[a]	−117.376	33.993	−17.4	11.6	0.07	0.06	0.34	25
RXH	−115.623	33.183	−17.4	16.4	0.08	0.02	0.51	5
SAL	−115.986	33.28	−5.3	16.0	0.06	0.06	0.52	5
SES	−119.137	34.437	−50.8	17.5	0.08	0.04	0.53	4
SLR[a]	−116.797	33.834	−53.0	6.8	0.07	0.05	0.37	60
SMS	−118.456	34.014	−4.3	33.3	0.1	0.05	0.14	19
SND[a]	−116.613	33.552	1.0	3.8	0.07	0.05	0.36	208
SSW[a]	−115.616	33.178	4.0	11.2	0.07	0.05	0.29	37
SVD	−117.098	34.106	−25.7	44.5	0.1	0.04	0.16	8
TRO[a]	−116.426	33.523	−41.8	13.3	0.07	0.05	0.25	36
USC[a]	−118.286	34.019	−23.9	11.9	0.07	0.03	0.55	8
WES	−115.732	32.759	−5.5	12.6	0.05	0.04	0.63	5
WGR[a]	−119.274	34.511	−51.3	5.7	0.04	0.02	0.87	7
WMC[a]	−116.675	33.574	−9.3	4.9	0.1	0.04	0.55	48
YAQ[a]	−116.354	33.167	−35.1	6.3	0.08	0.06	0.67	17

[a]A significant preferred direction of 90% confidence level.

They are nearly orthogonal to the stress directions from the World Stress Map and different from the absolute plate motion direction of North America (Figure 5). The time delays of SKS splitting are mainly caused by mantle anisotropy because they are too large to be explained with crustal anisotropy. The time delays of crustal anisotropy in southern California generally are less than 0.2 s [e.g., *Aster et al.*, 1990; *Li et al.*, 1994] with few measurements up to 0.3 s [*Cochran et al.*, 2003]. Three stations in our study area (SVD, PFO, and LAC) have been hypothesized to have double-layer anisotropy [*Özalaybey and Savage*, 1995], with the anisotropy in an upper lithospheric layer having different orientation than the anisotropy in the underlying asthenosphere. Our result at station SVD has a diverse distribution of fast directions and would not contribute much to the upper layer inferred from SKS anisotropy (Figures 3 and 5). The fast directions of upper crustal anisotropy at station PFO show considerable scatter but are at least roughly consistent with the fast direction of the SKS upper layer at PFO, but the time delay of upper crustal anisotropy is 0.06 s, much less than the 0.6 s measured by *Özalaybey and Savage* [1995] for the upper layer below PFO.

[22] One possible cause for SKS fast directions perpendicular to the directions of regional stress in southern California is that mantle minerals are aligned in response to Cenozoic tectonic stress [*Polet and Kanamori*, 2002; *Liu et al.*, 1995]. Another is that the SKS fast directions may be the consequence of a remnant subduction fabric [e.g., *Özalaybey and Savage*, 1995]. Recent studies of anisotropy in the crust and upper mantle seem to favor the latter explanation. Surface wave studies [*Lin et al.*, 2009, 2011] have shown that the patterns of anisotropy between the crust and uppermost mantle beneath southern California are different, inferring stratification of anisotropy with depth. Lower crustal

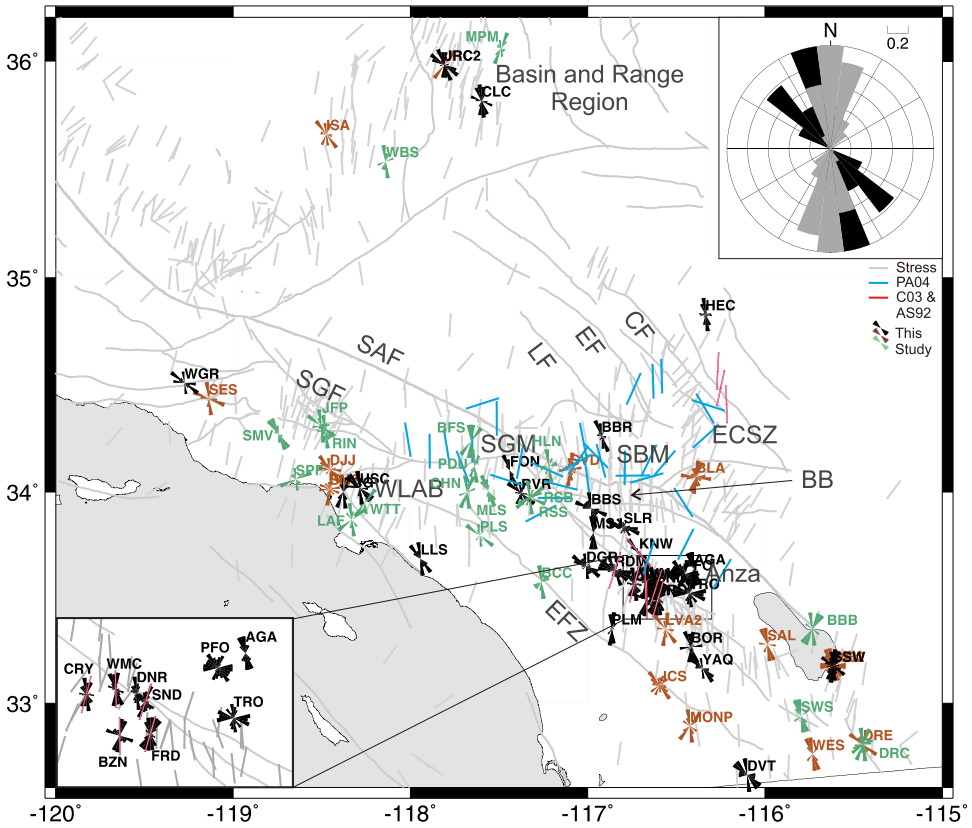

Figure 4. Map showing rose diagrams of the fast directions for each station (see details in Figure 2). Rose diagrams of stations with a ≥90% confidence level for a significant direction are in black. Brown rose diagrams are for stations with a confidence level less than 90%. Green rose diagrams are for those stations whose measurements have a cross-correlation coefficient less than 0.7. Red bars are fast orientations from previous studies of upper crustal anisotropy using local earthquakes with incident angles less than 45° [*Aster and Shearer*, 1992; *Cochran et al.*, 2003], and blue bars are the fast orientations from *Paulssen* [2004], which used earthquakes with incident angles larger than 45°. The bottom left corner shows an expanded view of the boxed area. Gray bars represent orientations of the axis of maximum horizontal compression in southern California, which are determined from borehole breakouts, hydraulic fracturing experiments, and earthquake focal mechanism inversions (World Stress Map Project). The inset rose diagram in the top right corner summarizes the orientation of σ_{Hmax} (gray) in the study region and the orientation of averaged fast directions for each seismic station with a 90% confidence level of a significant preferred direction to avoid emphasis on stations with large numbers of measurements (black). The two sets of orientations show a consistent range of directions of about 30° to −30°. BB, Big Bend (Banning Pass); CF, Calico Fault; ECSZ, east California shear zone; EF, Emerson Fault; EFZ, Elsinore Fault zone; LF, Lenwood Fault; SBM, San Bernadino Mountains; SGF, San Gabriel Fault; SGM, San Gabriel Mountains; WLAB, west Los Angeles basin.

anisotropy inferred from receiver functions also does not show a preferred direction, inconsistent with the southern California SKS results (R. Porter et al., Pervasive lower crustal seismic anisotropy in southern California: Evidence for underplated schists, submitted to *Lithosphere*, 2010).

[23] Overall, the fast directions of our upper crustal anisotropy observations do not coincide with either the directions of lower crustal anisotropy or the SKS measurements (Figure 5). In the shallow crust, our new anisotropy results seem to be mainly affected by the regional tectonic stress. In the lower crust, the anisotropy may come from the subcreted schist during Farallon plate subduction (Porter et al., submitted manuscript, 2010). The mantle anisotropy is most likely a remnant subduction fabric as discussed above.

4.3. Temporal Variations?

[24] There has been a debate on the possibility of using temporal variations of crustal anisotropy to predict earthquakes [e.g., *Aster et al.*, 1990; *Crampin et al.*, 1990; *Aster and Shearer*, 1991; *Crampin et al.*, 1991; *Munson et al.*, 1995; *Crampin et al.*, 1999], since cracks that can cause anisotropy may be sensitive to any stress changes that may occur before earthquakes [*Gupta*, 1973a, 1973b; *Crampin*, 1978, 1987; *Crampin et al.*, 1980, 1984]. Recent work by *Gerst and Savage* [2004] showed a change of fast direction in local earthquake shear wave splitting before and after volcanic eruptions, suggesting that stress changes in and around magma chambers can be monitored. For stress changes associated with earthquakes, *Saiga et al.* [2003]

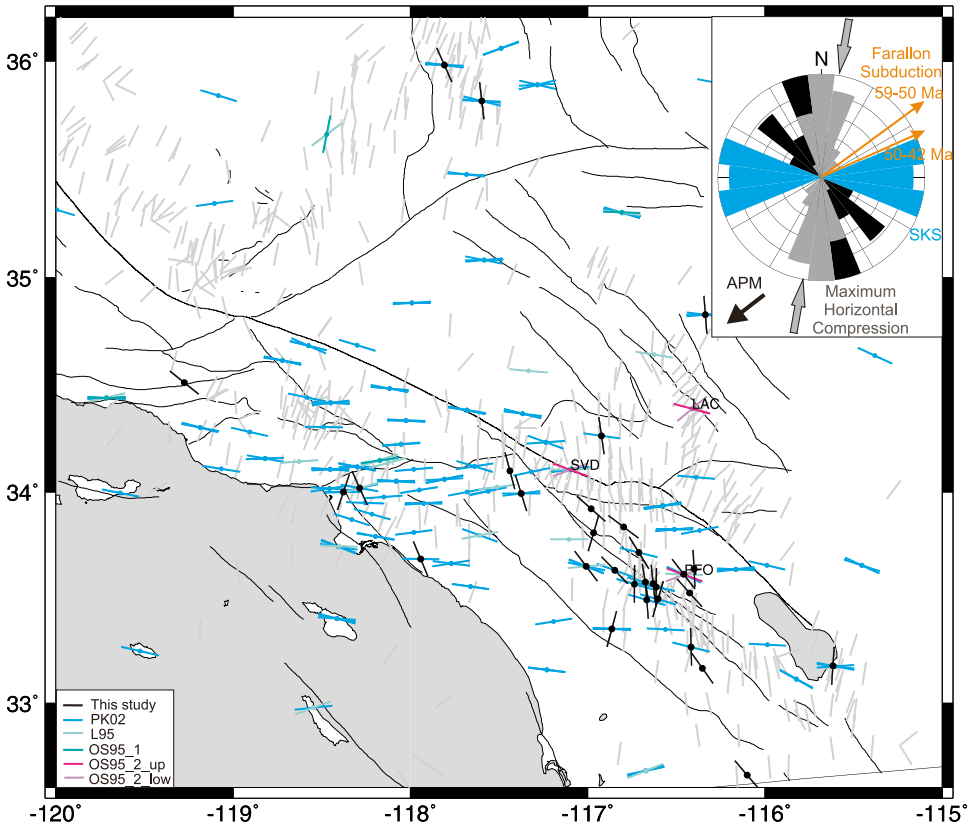

Figure 5. Map showing average fast directions of upper crustal anisotropy (solid bars) for the stations having significant preferred directions at the 90% confidence level, SKS shear wave splitting anisotropy (see legend), and stress vectors (gray bars). The inset rose diagram summarizes the trends of anisotropies from three different depths in the area of the map: top 20 km of crust (black), the fast directions are consistent with the direction of current maximum horizontal compression (gray arrows); and upper mantle, SKS shear wave splitting show a preferred fast direction orienting E–W (blue bars). The orange arrows are Farallon plate subduction directions during 59–42 M_a [*McQuarrie and Wernicke*, 2005]. The trends of anisotropy in the lower crust (below 20 km), after correcting the plate rotations in the past 36 M_a [Porter et al., submitted manuscript, 2010], are consistent with the Farallon subduction directions during 59–42 M_a. The black arrow indicates the absolute plate motion (APM) of the North American plate [*Gripp and Gordon*, 1990].

claimed that they observed temporal changes of crustal anisotropy due to coseismic stress changes for a moderate-sized earthquake (M 5.7) in the Tokai region, central Japan. *Tadokoro et al.* [1999] suggested that local earthquake shear wave splitting could be used to monitor postseismic fault healing because they observed spatial variations in the orientation of cracks or fractures in and around the aftershock region of 1995 Hyogo-Ken Nambu earthquake (Kobe earthquake, M 7.2). However, results from *Peng and Ben-Zion* [2004] did not show systematic precursory changes before the 1999 Düzce main shock (M_w 7.1) along the North Anatolian Fault, and *Liu et al.* [2008] did not observe any temporal variations in local earthquake shear wave anisotropy around the San Andreas Fault near Parkfield.

[25] To explore the possible time variation of the upper crustal anisotropy in southern California between 2000 and 2005, we examine five stations with the most data (over 100 measurements) and present two examples (KNW and CRY) in Figure 6. The measurements exhibit large scatter (Figure 6) without any clear temporal trends. Measurements exceeding 2 standard deviations do not correlate with specific back azimuths, incident angles, or focal depths of events. Without being able to definitely reject these outliers, we apply moving averages both to all data points (Figure 6, green curve) and data points within 2 standard deviations (Figure 6, pink). We have tried 10-, 20-, and 30-point moving averages, which all produce similar results (Figure 6 shows only the 10-point moving average curve). Although there is a hint of a change in the moving average curve following the first of these events, we do not observe any systematic association between the occurrences of earthquakes and the smoothed variations (moving averages) of the fast directions and time delays. For all five of the stations we examined, we do not observe any clear or consistent temporal variations in anisotropy associated with earthquake occurrence.

5. Conclusions

[26] We have measured anisotropy in the southern California upper crust (top 20 km) using local earthquake shear wave splitting. The fast directions at most stations are consistent with the local stress orientation, suggesting that the

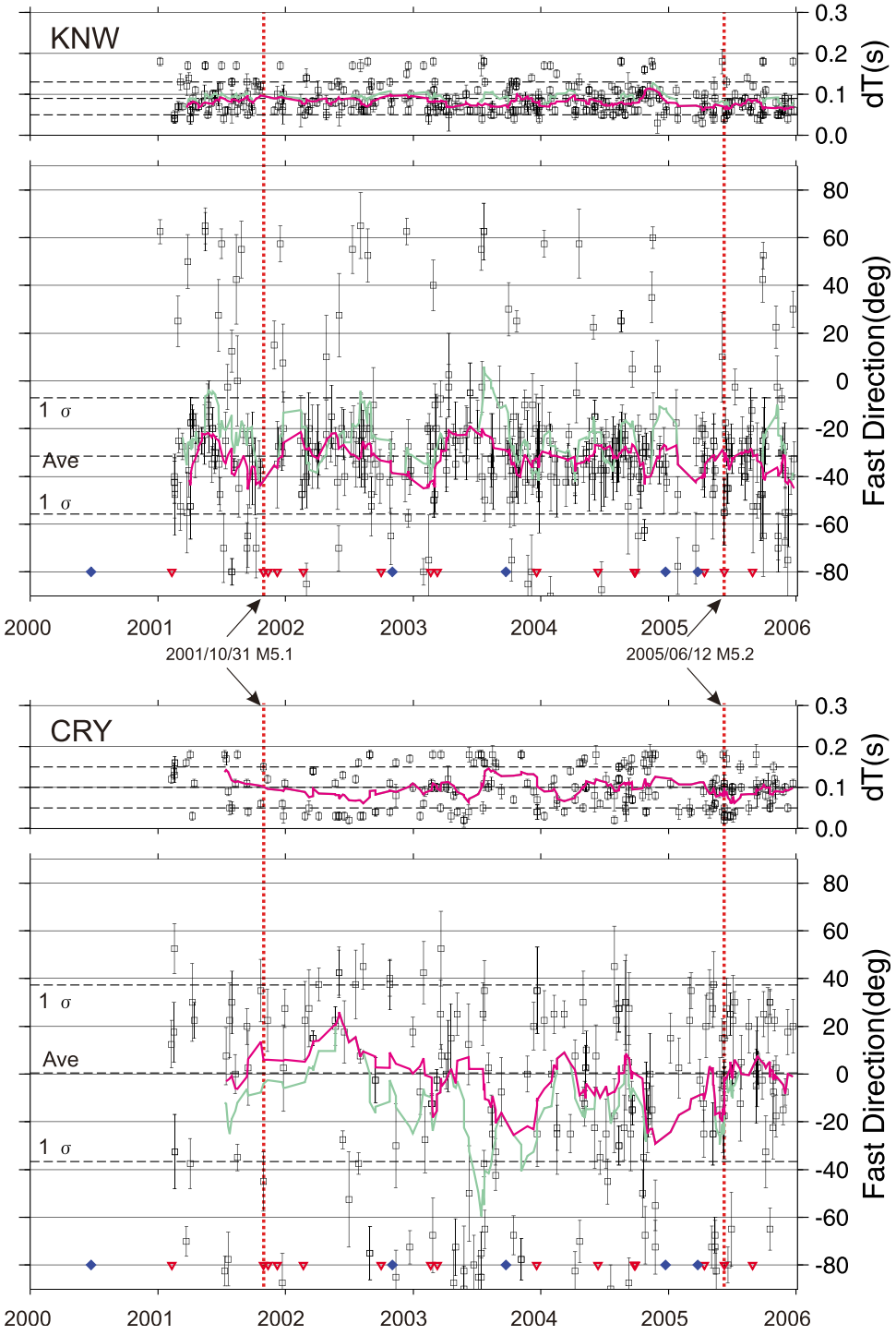

Figure 6. Examples of fast directions and time delays as a function of time at stations KNW and CRY. Red inverted triangles and blue diamonds mark the origin times of local earthquakes larger than magnitude 5.0 and global great earthquakes ($M > 7.0$) at teleseismic distances, respectively. In particular, red dotted lines highlight the origin times of $M \sim 5$ events on 30 October 2001 and 12 June 2005, which took place near the Anza region, less than 30 km away from stations CRY and KNW. Around the times of these two events, no dramatic changes in either delay times or fast directions are observed.

anisotropy in the top 20 km is mainly caused by preferentially aligned cracks responding to the stress field, although local structures and structural fabrics can also affect the anisotropy. Our results, together with previous studies of anisotropy in the lower crust and mantle, indicate depth-varying anisotropy under southern California. The anisotropy in the upper crust, lower crust, and mantle exhibit different mechanisms of anisotropy and are involved with

different tectonic processes. Our results show no distinctive temporal variations in shear wave splitting time delays or fast directions between 2000 and 2005.

[27] **Acknowledgments.** The data used in this study were made available by the Southern California Seismic Network, and we are grateful to E. Hauksson for his assistance in creating a waveform database. We thank J. Polet for providing a digital table of his Southern California SKS measurements, R. Porter for sharing a preprint of his Southern California receiver function work, and M. Savage for her comments. The figures were made using GMT software by P. Wessel and W. Smith. A.S. gratefully acknowledges a Green Foundation Fellowship that supported her sabbatical at IGPP/SIO. This work is supported by SCEC project 08129 and NSF EAR grant 0409835 and by U.S. Geological Survey award G09AP00052.

References

Abers, G. A., and J. W. Gephart (2001), Direct inversion of earthquake first motions for both the stress tensor and focal mechanisms and applications to southern California, *J. Geophys. Res.*, *106*(B11), 26,523–26,540, doi:10.1029/2001JB000437.

Aster, R. C., and P. Shearer (1991), High-frequency borehole seismograms recorded in the San Jacinto fault zone, Southern California, Part 1: Polarizations, *Bull. Seismol. Soc. Am.*, *81*, 1057–1080.

Aster, R. C., and P. M. Shearer (1992), Initial shear wave particle motions and stress constraints at the Anza Siesmic Network, *Geophys. J. Int.*, *108*, 740–748, doi:10.1111/j.1365-246X.1992.tb03465.x.

Aster, R. C., P. M. Shearer, and J. Berger (1990), Quantitative measurements of shear wave polarizations at the Anza seismic network, southern California: Implications for shear wave splitting and earthquake prediction, *J. Geophys. Res.*, *95*(B8), 12,449–12,473, doi:10.1029/JB095iB08p12449.

Boness, N. L., and M. D. Zoback (2004), Stress-induced seismic velocity anisotropy and physical properties in the SAFOD pilot hole in Parkfield, CA, *Geophys. Res. Lett.*, *31*, L15S17, doi:10.1029/2003GL019020.

Boness, N. L., and M. D. Zoback (2006), A multiscale study of the mechanisms controlling shear velocity anisotropy in the San Andreas Fault Observatory at Depth, *Geophysics*, *71*(5), doi:10.1190/1.2231107.

Booth, D. C., and S. Crampin (1985), Shear-wave polarizations on a curved wave front at an isotropic free surface, *Geophys. J. R. Astron. Soc.*, *83*, 31–45.

Brocher, T., and N. Christensen (1990), Seismic anisotropy due to preferred mineral orientation observed in shallow crustal rocks in southern Alaska, *Geology*, *18*, 737–740, doi:10.1130/0091-7613(1990)018<0737:SADTPM>2.3.CO;2.

Cochran, E. S., J. E. Vidale, and Y.-G. Li (2003), Near-fault anisotropy following the Hector Mine earthquake, *J. Geophys. Res.*, *108*(B9), 2436, doi:10.1029/2002JB002352.

Cochran, E., Y.-G. Li, and J. Vidale (2006), Anisotropy in the shallow crust observed around the San Andreas Fault before and after the 2004 M 6.0 Parkfield earthquake, *Bull. Seismol. Soc. Am.*, *96*, S364–S375, doi:10.1785/0120050804.

Crampin, S. (1978), Siesmic-wave propagation through a cracked solid: Polarization as a possible dilatancy diagnostic, *Geophys. J. R. Astron. Soc.*, *53*, 467–496.

Crampin, S. (1986), Anisotropy and transverse isotropy, *Geophys. Prospect.*, *34*, 94–99, doi:10.1111/j.1365-2478.1986.tb00454.x.

Crampin, S. (1987), Geological and industrial implications of extensive dilatancy anisotropy, *Nature*, *328*, 491–496, doi:10.1038/328491a0.

Crampin, S., R. Evans, B. Ucer, M. Doyle, J. P. Davis, G. V. Yegorkina, and A. Miller (1980), Observations of dilatancy-induced polarization anomalies and earthquake prediction, *Nature*, *286*, 874–877, doi:10.1038/286874a0.

Crampin, S., R. Evans, and B. K. Atkinson (1984), Earthquake prediction: A new physical basis, *Geophys. J. R. Astron. Soc.*, *76*, 147–156.

Crampin, S., D. C. Booth, R. Evans, S. Peacock, and J. B. Fletcher (1990), Change in shear wave splitting at Anza near the time of the North Palm Springs earthquake, *J. Geophys. Res.*, *95*, 11,197–11,212, doi:10.1029/JB095iB07p11197.

Crampin, S., D. C. Booth, R. Evans, S. Peacock, and J. B. Fletcher (1991), Comment on "Quantitative measurements of shear wave polarizations at the Anza seismic network, southern California: Implications for shear wave splitting and earthquake prediction" by R. C. Aster, P. M. Shearer, and J. Berger, *J. Geophys. Res.*, *96*, 6403–6414, doi:10.1029/90JB02453.

Crampin, S., T. Volti, and R. Stefansson (1999), A successfully stress-forecast earthquake, *Geophys. J. Int.*, *138*, F1–F5, doi:10.1046/j.1365-246x.1999.00891.x.

Davis, J. C. (1986), *Statistics and Data Analysis in Geology*, 646 pp., John Wiley, Hoboken, N. J.

Gerst, A. (2003), Temporal changes in seismic anisotropy as a new eruption forecasting tool? M.Sc. thesis, Victoria Univ. of Wellington, New Zealand.

Gerst, A., and M. K. Savage (2004), Seismic anisotropy beneath Ruapehu volcano: A possible eruption forecasting tool, *Science*, *306*, 1543–1547, doi:10.1126/science.1103445.

Gripp, A. E., and R. G. Gordon (1990), Current plate velocities relative to the hotspots incorporating the NUVEL-1 global plate motion model, *Geophys. Res. Lett.*, *17*(8), 1109–1112, doi:10.1029/GL017i008p01109.

Gupta, I. N. (1973a), Dilatancy and premonitory variations of P, S travel times, *Bull. Seismol. Soc. Am.*, *63*, 1157–1161.

Gupta, I. N. (1973b), Premonitory variations in S wave velocity anisotropy before earthquakes in Nevada, *Science*, *182*, 1129–1132, doi:10.1126/science.182.4117.1129.

Hauksson, E., and P. Shearer (2006), Attenuation models (Qp and Qs) in three dimensions of the southern California crust: Inferred fluid saturation at siesmogenic depths, *J. Geophys. Res.*, *111*, B05302, doi:10.1029/2005JB003947.

Heidbach, O., M. Tingay, A. Barth, J. Reinecker, D. Kurfeß, and B. Müller (2008), The World Stress Map database release 2008, doi:10.1594/GFZ.WSM.Rel2008.

Jennings, C. W. (1994), Fault activity map of California and adjacent areas, *Data Map Ser. 6*, 92 p., scale 1:750,000, Calif. Div. of Mines and Geol., Sacramento.

Kern, H., and H.-R. Wenk (1990), Fabric-related velocity anisotropy and shear wave splitting in rocks from the Santa Rosa Mylonite Zone, California, *J. Geophys. Res.*, *95*, 11,213–11,223, doi:10.1029/JB095iB07p11213.

Leary, P. C., S. Crampin, and T. McEvilly (1990), Seismic fracture anisotropy in the earth's crust: An overview, *J. Geophys. Res.*, *95*, 11,105–11,114, doi:10.1029/JB095iB07p11105.

Li, Y.-G., T.-L. Teng, and T. L. Henyey (1994), Shear-wave splitting observations in the northern Los Angeles Basin, southern California, *Bull. Seismol. Soc. Am.*, *84*(2), 307–323.

Lin, F.-C., M. H. Ritzwoller, and R. Snieder (2009), Eikonal tomography: Surface wave tomography by phase front tracking across a regional broad-band seismic array, *Geophys. J. Int.*, *177*, 1091–1110, doi:10.1111/j.1365-246X.2009.04105.x.

Lin, F.-C., M. H. Ritzwoller, Y. Yang, M. Moschetti, and M. Fouch (2011), Complex and variable crustal and uppermost mantle seismic anisotropy in the western United States, *Nat. Geosci.*, *4*, 55–61, doi:10.1038/ngeo1036.

Liu, H., P. M. Davis, and S. Gao (1995), SKS splitting beneath southern California, *Geophys. Res. Lett.*, *22*, 767–770, doi:10.1029/95GL00487.

Liu, Y., S. Crampin, and I. Main (1997), Shear-wave anisotropy: Spatial and temporal variations in time delays at Parkfield, central California, *Geophys. J. Int.*, *130*, 771–785, doi:10.1111/j.1365-246X.1997.tb01872.x.

Liu, Y., H. Zhang, C. Thurber, and S. Roecker (2008), Shear wave anisotropy in the crust around the San Andreas fault near Parkfield: Spatial and temporal analysis, *Geophys. J. Int.*, *172*, 957–970, doi:10.1111/j.1365-246X.2007.03618.x.

Mardia, K. V., and P. E. Jupp (2000), *Directional Statistics*, 429 pp., John Wiley, Hoboken, N. J.

McQuarrie, N., and B. P. Wernicke (2005), An animated tectonic reconstruction of southwestern North America since 36 Ma, *Geosphere*, *1*(3), 147–172, doi:10.1130/GES00016.1.

Miller, V., and M. K. Savage (2001), Changes in seismic anisotropy after volcanic eruptions: Evidence from Mount Ruapehu, *Science*, *293*, 2231–2233, doi:10.1126/science.1063463.

Munson, C. G., C. H. Thurber, Y.-G. Li, and P. G. Okubo (1995), Crustal shear wave anisotropy in southern Hawaii: Spatial and temporal analysis, *J. Geophys. Res.*, *100*(B10), 20,367–20,377, doi:10.1029/95JB01288.

Nuttli, O. (1961), The effect of earth's surface on the S-wave particle motion, *Bull. Seismol. Soc. Am.*, *107*, 409–415.

Özalaybey, S., and M. K. Savage (1995), Shear-wave splitting beneath western United States in relation to plate tectonics, *J. Geophys. Res.*, *100*(B9), 18,135–18,149, doi:10.1029/95JB00715.

Paulssen, H. (2004), Crustal anisotropy in southern California from local earthquake data, *Geophys. Res. Lett.*, *31*, L01601, doi:10.1029/2003GL018654.

Peacock, S., S. Crampin, D. C. Booth, and J. B. Fletcher (1988), Shear wave splitting in the Anza seismic gap, southern California: Temporal variations as possible precursors, *J. Geophys. Res.*, *93*, 3339–3356, doi:10.1029/JB093iB04p03339.

Peng, Z., and Y. Ben-Zion (2004), Systematic analysis of crustal anisotropy along the Karadere-Duzce branch of the North Anatolian fault, *Geophys. J. Int.*, *159*, 253–274, doi:10.1111/j.1365-246X.2004.02379.x.

Polet, J., and H. Kanamori (2002), Anisotropy beneath California: Shear wave splitting measurements using a dense broadband array, *Geophys. J. Int.*, *149*, 313–327, doi:10.1046/j.1365-246X.2002.01630.x.

Saiga, A., Y. Hiramatsu, T. Ooida, and K. Yamaoka (2003), Spatial variation in the crustal anisotropy and its temporal variation associated with a moderate-sized earthquake in the Tokai region, central Japan, *Geophys. J. Int.*, *154*, 695–705, doi:10.1046/j.1365-246X.2003.01998.x.

Savage, M. K., W. A. Peppin, and U. R. Vetter (1990), Shear wave anisotropy and stress direction in and near Long Valley Caldera, California, 1979–1988, *J. Geophys. Res.*, *95*, 11,165–11,177, doi:10.1029/JB095iB07p11165.

Savage, M. K., T. Ohminato, Y. Aoki, H. Tsuji, and S. M. Greve (2010), Stress magnitude and its temporal variation at Mt. Asama Volcano, Japan, from seismic anisotropy and GPS, *Earth Planet. Sci. Lett.*, *290*, 403–414, doi:10.1016/j.epsl.2009.12.037.

Shearer, P. M., G. A. Prieto, and E. Hauksson (2006), Comprehensive analysis of earthquake source spectra in southern California, *J. Geophys. Res.*, *111*, B06303, doi:10.1029/2005JB003979.

Silver, P. G., and W. J. Chan (1991), Shear-wave splitting and subcontinental mantle deformation, *J. Geophys. Res.*, *96*, 16,429–16,454, doi:10.1029/91JB00899.

Tadokoro, K., M. Ando, and Y. Umeda (1999), S wave splitting in the aftershock region of the 1995 Hyogo-ken Nanbu earthquake, *J. Geophys. Res.*, *104*, 981–991, doi:10.1029/1998JB900024.

Teanby, N. A., J.-M. Kendall, and M. van der Bann (2004), Automation of shear-wave splitting measurements using cluster analysis, *Bull. Seismol. Soc. Am.*, *94*(2), 453–463, doi:10.1785/0120030123.

Townend, J., and M. D. Zoback (2004), Regional tectonic stress near the San Andreas fault in central and southern California, *Geophys. Res. Lett.*, *31*, L15S11, doi:10.1029/2003GL018918.

P. Shearer, IGPP 0225, Scripps Institution of Oceanography, La Jolla, CA 92093-0225, USA.

A. Sheehan and Z. Yang, Cooperative Institute for Research in Environmental Sciences, University of Colorado at Boulder, Bensen Earth Science Building, Boulder, CO 80309-0399, USA. (zhaohui.yang@colorado.edu)